Accepted Manuscript

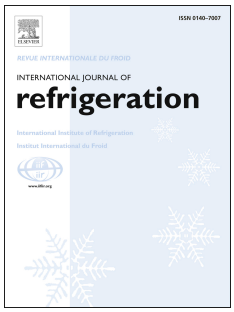

Analysis of heat transfer phenomena during ice slurry production in scraped surface plate heat exchangers

David S. Martínez, Juan P. Solano, Fernando Illán, Antonio Viedma

PII: S0140-7007(14)00198-4

DOI: 10.1016/j.ijrefrig.2014.07.020

Reference: JIJR 2845

To appear in: *International Journal of Refrigeration*

Received Date: 6 February 2014

Revised Date: 19 July 2014

Accepted Date: 22 July 2014

Please cite this article as: Martínez, D.S., Solano, J.P., Illán, F., Viedma, A., Analysis of heat transfer phenomena during ice slurry production in scraped surface plate heat exchangers, International Journal of Refrigeration (2014), doi: 10.1016/j.ijrefrig.2014.07.020.

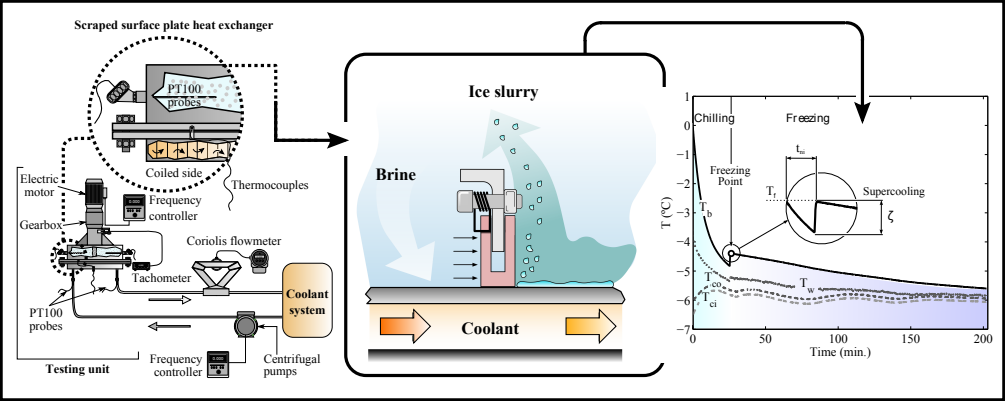
Scraped surface plate heat exchanger
PT100 probes
Coiled side
Thermocouples
Electric motor
Frequency controller
Gearbox
Coriolis flowmeter
Tachometer
Coolant system
PT100 probes
Testing unit
Frequency controller
Centrifugal pumps
Ice slurry
Brine
Coolant
Chilling
Freezing
Freezing Point
Supercooling
T (°C)
Time (min.)

Title page

Article title: Analysis of heat transfer phenomena during ice slurry production in scraped surface plate heat exchangers

Journal: *International Journal of Refrigeration*

Author: David S. Martínez

Universidad Politécnica de Cartagena. Dep. Ingeniería Térmica y de Fluidos.
c/ Dr. Fleming s/n
30202 Cartagena (Murcia), Spain
Phone: +34 968 32 59 94
FAX: +34 968 32 59 99
davids.martinez@upct.es

Co-author: Juan P. Solano

Universidad Politécnica de Cartagena. Dep. Ingeniería Térmica y de Fluidos.
c/ Dr. Fleming s/n
30202 Cartagena (Murcia), Spain
Phone: +34 968 32 59 38
FAX: +34 968 32 59 99
juanp.solano@upct.es

Co-author: Fernando Illán

Universidad Politécnica de Cartagena. Dep. Ingeniería Térmica y de Fluidos.
c/ Dr. Fleming s/n
30202 Cartagena (Murcia), Spain
Phone: +34 968 32 59 95
FAX: +34 968 32 59 99
fernando.illan@upct.es

Co-author: Antonio Viedma

Universidad Politécnica de Cartagena. Dep. Ingeniería Térmica y de Fluidos.
c/ Dr. Fleming s/n
30202 Cartagena (Murcia), Spain
Phone: +34 968 32 59 81
FAX: +34 968 32 59 99
antonio.viedma@upct.es

Abstract

Heat transfer during ice slurry production in a scraped surface plate heat exchanger (SSPHE) has been experimentally investigated. By using a 7 wt. % sodium chloride brine, a wide range of operating conditions has been tested: scraping velocities from 0.1 to 0.8 s^{-1} and logarithmic temperature differences from 0.5 to 2.5 °C. Two different PEEK scraper arrangements have been used, mounted on the driving arms: rigid scrapers and surface adaptable scrapers, pushed by torsion springs. Heat transfer coefficients and ice production rate were measured under batch operating mode. Experimental results shown dependence of the nucleation onset with the scraping speed and the wall supercooling degree. Global nucleation only occurred for high velocities and low supercooling degrees, appearing only on the wall for the other cases. A decrease of the heat transfer coefficient of 1.5 times for increasing logarithmic temperature differences is reported, as a consequence of the ice layer growth with a low effect of the scraping speed. The use of adaptable scrapers provide heat transfer coefficient augmentations from 2 to 4-fold with respect to the rigid configuration.

Keywords: ice slurry , scraped surface , heat exchanger , heat transfer enhancement , active techniques

Nomenclature

A	heat exchange area (m^2)
C	constant term (W m^{-2} K^{-1})
D	SSPHE internal diameter (m)
H	SSPHE internal height (m)
H_S	scraper height (m)
L_f	ice specific latent heat of fusion at 0 °C (J)
N	rotational speed (s^{-1})
Q	heat flux (W)
T	temperature (° C)
V	volume of the heat exchanger (m^3)
$\dot{m}$	coolant mass flow (kg s^{-1})
$\hat{c}_p$	specific heat (J kg^{-1} K^{-1})
c_p	specific heat (J kg^{-1} K^{-1})
e	ice layer thickness (m)
g	gravity acceleration (m s^{-2})
h	heat transfer coefficient (W m^{-2} K^{-1})
i	specific enthalpy (J kg^{-1} K^{-1})
k	thermal conductivity (W m^{-1} K^{-1})
n	number of scrapers
t	time (s)
t_{ni}	nucleation induction time (s)
v	coolant velocity (m/s^{-1})

Dimensionless numbers	
Fr	Froude number $\Omega\ D/2\ ^2/Hg\ 1-\rho_i/\rho_b$
Nu	Nusselt number hD/k
Pr	Prandtl number $\mu c_p/k$
Re	Reynolds number $\rho vD/\mu$
Re_{rot}	rotative Reynolds number $\rho ND^2/\mu$
Ri	Richardson number $g\beta\Delta T_{b,w}\ H/2\ /\ \Omega\ D/2\ ^2$
Greek symbols	
β	thermal expansion coefficient (°C^{-1})
ΔT_s	wall supercooling degree $T_f - T_w$ (° C)
ΔT_{log}	logarithmic mean temperature diff. (° C)
μ	viscosity (kg m^{-1} s^{-1})
Ω	rotor angular velocity (rad s^{-1})
ω	solute mass fraction in the brine; mass of NaCl/mass of solution
ω_0	global mass fraction of solute; mass of NaCl/mass of solution and ice
ρ	density (kg m^{-3})
φ_m	ice mass fraction
φ_v	ice volume fraction
Φ	viscous dissipation term (W)
ζ	supercooling amplitude (° C)
Subscripts	
b	brine
c	coolant
e	inlet
F	final
f	freezing
i	ice
max	maximum
o	outlet
p	process
s	subcooling
w	wall

0	initial
n	n^{th} element
calc	calculated
exp	experimental
T	total

1. Introduction

Ice slurries have a wide range of applications, being involved from food processing to water purification processes, with an special relevance on refrigeration and energy storage. The high cooling capacity and constant cooling temperature, together with their easy transportability make the ice slurries a suitable coolant. Among the different techniques available for the production of ice slurries [1], the scraper type systems and particularly the scraper surface heat exchangers (SSHE) deserve an special interest. Their ability for the fouling prevention is applied here for the continuous removal of the ice layer, generating small ice crystals and adding them to the mixture. Moreover the continuous removal of the boundary layer enhances the heat transfer between the wall and the surrounding fluid.

The aim of the present work is the experimental study of the ice slurry generation in a SSPHE working in batch mode. An analysis of the phase-change heat transfer process that occurs during the ice slurry generation is presented, based on the appropriate parameters and dimensionless numbers that help describe the involved phenomena. A through characterization of the heat transfer to the scraped-surface wall is accounted for by means of the influence of various parameters (blade rotation speed, type of scrapers, wall supercooling degree, product concentration) for a 7 wt. % wt. NaCl brine. We propose design correlations able to predict the heat transfer at a scraped surface when freezing of water occurs.

1.1. Literature review

Heat transfer in SSHEs, mostly regarding horizontal models –where an inner cylindrical surface is continuously scraped by means of rotating blades– have been widely investigated [2]. One of the most extensively used models for describing heat transfer in SSHEs uses the *penetration theory*. Although several researchers have questioned its validity in the transition and turbulent region [3, 4], other studies confirmed that liquids having low viscosity could be adequately described using the penetration theory [5], and it has been subsequently modified to include the effects of parameters such as rotation and number of blades [6].

Several investigations have been reported in the open literature on the production of ice slurries in SSHEs. Qin et al [7] used an horizontal scraped surface plate heat exchanger (SSPHE) and described the three stages in which the formation of the ice slurry occurs: chilling, nucleation and crystallization. The authors observed increased heat transfer coefficients for the stage with crystallization, arguing that although crystal formation on the cooling surface is considered disadvantageous to heat transfer, liberation of latent heat of crystallization on the cooling surface actually increased the heat transfer.

The same authors reported afterwards a study on the heat transfer and power consumption in a SSHE while freezing aqueous solutions [8] and on the ice fouling on a subcooled metal surface [9]. They found that the reduction of the cooler surface supercooling degree may delay the ice fouling and prolong the induction time or even perhaps avoid it. However they did not measure the temperatures at the subcooled wall.

The effect of the electrolyte concentration and the scraping speed have been studied by Vaessen et al [10], who compared two types of scraped surface heat exchangers (cooled column disc and scraper cooled wall). The authors found that for both designs the transport of heat from process liquid to cooled wall surfaces (without phase change) at various rotational speeds of the scrapers can be accurately described by the penetration theory, expressed as

$$\bar{h} = 2\sqrt{\frac{\rho \cdot c_p \cdot k \cdot n \cdot N}{\pi}} \quad (1)$$

and assessing its applicability also to the phase change. However they did not calculate the thermophysical properties of the slurry and therefore not direct comparisons with the penetration theory were presented during the phase change. As a major conclusion, the authors observed that the increase of ice content in the crystallizer probably dominates over the increase of the scraping speed, decreasing the process-side heat transfer with higher temperature differences and scraping rates.

In general, the behaviour of the SSHEs when used for crystallization processes can be characterized by the induction time, defined as the maximum interim value between two ice removal actions of the scraper. Anew Vaessen [11] investigated the phenomenon of ice scale formation on subcooled surfaces, finding that higher supercooling degrees led to lower induction times, whereas the opposite was found regarding the electrolyte solute content. Qin et al [12] obtained a similar conclusion, finding that the fouling induction time is mainly determined by the degree of wall supercooling. Therefore, a constant presence of a thin ice layer can be assumed, due to the inefficacy of the scrapers to remove it completely, whereas the scale formation is only avoidable by a real mechanical removal, entailing a sudden decrease on heat transfer.

Further studies have been carried out on the SSHE for ice slurry production considering tubular geometries, mostly with rotating blades [13, 14]. Stamatiou [15] summarized the available Nusselt number correlations for this type of systems. However, and due to the complex fluid mechanical and heat transfer phenomena occurring in such systems, there has not been any meaningful heat transfer correlations based on the physical phenomena during the forced-convective crystallization involving phase change and agitation. The design of SSHEs for ice slurry generation does not attend to general guides, depending mostly on the operating conditions.

2. Material and methods

2.1. Experimental setup

A schematic diagram of the experimental set-up is presented in Fig. 1. The heat exchanger (ice slurry production unit) consists of a $28 \cdot 10^{-3}$ m^3 AISI 316 tank of 0.6 m diameter and 0.1 m height with a scraped heat transfer surface at the bottom. A 7 wt. % sodium chloride brine, accurately measured by a conductivity meter, is employed as the base solution for the generation of ice slurries in a batch process. The heat transfer surface is cooled underneath by a constant flow of calcium chloride solution in water (25 wt. %, Q=1.5 kg/s, -9 ºC$< T_c <$ -4 ºC), which flows across a coiled circuit (Fig. 2). The coolant solution is subsequently cooled by the expansion of a flow of R507 refrigerant in a compact evaporator. A damping tank of 0.3 m^{-3} is used to avoid instabilities in the coolant temperature. The compressor operating regime is settled by a frequency converter regulated by a PID controller, providing a constant coolant temperature during the running of the experiment.

Regularly distributed thermocouples are embedded in the rear side of the heat transfer plate (see Fig. 3) with an accuracy of $\pm$ 0.3 ºC. They provide an indirect measurement of the wall temperature in the scraped surface, while four immersed PT-100 sensors placed 90° apart circumferentially at 50 mm of height retrieve the bulk fluid temperature of the NaCl brine in the SSPHE upper side. The heat transfer to the cooling circuit is accounted for with PT-100 sensors which measure the inlet and outlet temperature of the coolant flow, whereas a Coriolis flow meter is used for obtaining the mass flow rate of coolant. The heat exchanger and the coolant tubes are fully insulated by an elastomeric thermal insulation material of 30 mm thickness and thermal conductivity 0.04 W/(m·K), in order to minimize heat losses to the ambient. Wall temperature measurements under the most unfavorable conditions reported maximum losses of 4% respect to the heat exchanged inside the SSPHE.

The coolant mass flow proved to be high enough to minimize the temperature differences across the heat transfer plate, were the maximum found standard deviation among them was of $\approx$ 0.2 ºC.

The scraper system is composed of four rotating blades –90° apart circumferentially– driven by a rotating shaft. A frequency controlled electrical motor is connected to the shaft through a gearbox. The power consumed by the motor is measured by a wattmeter, placed between it and the frequency converter. Each blade is made of a steel arm where the actual scrapers are mounted. The scraper are made of PEEK, a polymer with high resistance to the erosion. Two different configurations of scrapers where tested; rigid and adaptable. The first one consisted on single piece scrapers fixed to each steel arm, where the movement between the arm and the scraper was restricted. The second system (Fig. 2) employed three independent scrapers mounted on each arm. Each scraper device was connected to the arm by means of two torsion springs, which maximizes the contact between the scraper and the plate even if the latter loses its planar shape. The independent motion of the different scrapers, together with the force applied by the torsion springs, provide a high adaptability to the plate surface. The system can be observed in the sketch shown in Fig. 3.

Geometrical details of the experimental facility and operating conditions are summarized in Table 1.

2.2. Thermophysical properties and ice content

The thermopysical properties involved in the definition of the dimensionless numbers correspond to the ice slurry for the pertinent ice contents. Regarding the brine properties, the relations recommended by Melinder [16] were used for the density, viscosity, specific heat, thermal conductivity and freezing point temperature. Except during the supercooling, thermal equilibrium can be assumed with no solute in the ice crystals. Therefore the NaCl mass fraction can be determined by the temperature of the mixture from the liquidus curve,

$$\omega\ T_b\ = -0.004473T_b^2 - 1.6022T_b + 0.041643; \qquad (2)$$

where, in equilibrium, the slurry temperature is equal to the freezing point temperature $T_b = T_f\ \ \omega\ \Leftrightarrow \omega = \omega_f\ \ T_b\ \ .$

The global mass fraction of solute in the slurry ω_0 (kg solute/kg solution+ice)remains constant and equal to the value of ω before freezing. Since the initial NaCl mass fraction is known, the ice mass fraction in the slurry (kg ice/kg slurry) is calculated as,

$$\varphi_m = 1 - \frac{\omega_0}{\omega\ T_b} \qquad (3)$$

The slurry density is obtained by addition of ice and brine volume,

$$\frac{1}{\rho} = \frac{\varphi_m}{\rho_i} + \frac{1-\varphi_m}{\rho_b} \qquad (4)$$

The volume mass fraction of the ice slurry is then,

$$\varphi_v = \varphi_m \frac{\rho}{\rho_i} \qquad (5)$$

The thermal conductivity is obtained by the Maxwell lower bound relation [17] for dilute solid/ liquid suspensions,

$$k = k_b[\frac{2k_b + k_i - 2\varphi_v\ \ k_b - k_i}{2k_b + k_i + \varphi_v\ \ k_b - k_i}] \qquad (6)$$

where k_b and k_i are the thermal conductivities of the brine and ice and φ_v can be obtained from the slurry temperature.

The specific enthalpy of the slurry is obtained by those of ice and brine

$$i = \varphi_m \left(-L_f + \int_{0\,^\circ C}^{T_F} c_{p,i}\ T\ dT \right) + \left(1 - \varphi_m\right) \int_{0\,^\circ C}^{T_F} c_{p,b}\ T\ dT \qquad (7)$$

Since c_p is a function of the temperature as it is φ_m (through Eq. 2), the specific enthalpy will depend only on the temperature for a given solute mass fraction ω_0. An apparent specific heat can then be defined for the slurry (needed energy to increase by 1 K, 1 kg of slurry following the liquidus curve). This specific heat is hereafter used to calculate the Prandtl number.

$$\hat{c}_p = \frac{di}{dT} \qquad (8)$$

The ice slurry behaviour depends strongly on the ice content, and most of the authors agree that the limit between Newtonian and non-Newtonian behaviour is between 6 and 15% [18, 19]. The relation proposed by Thomas [20] for solid/liquid suspensions was used to calculate the dynamic viscosity as a function of the brine viscosity and the ice particle concentration

$$\mu = \mu_b \left(1 + 2.5\varphi_v + 10.05\varphi_v^2 + 0.00273 e^{16.6\varphi_v}\right) \qquad (9)$$

The above equation considers homogeneous and non Newtonian flow, and is commonly valid for solid phase concentrations up to 62.5% and for all particle sizes between 0.099 and 435 μm. However, for the particular case of ice slurries, the equation is limited to ice concentrations below 15%, Higher concentration values lead to viscosity values greater than the experimentally obtained.

2.3. Heat flux measurement

The heat flux exchanged through the surface was estimated by a heat balance in the heat exchanger. Assuming negligible losses to the ambient and neglecting viscous dissipation effects, the heat lost by the slurry is gained by the coolant flow. Since inlet and outlet coolant temperatures together with its mass flow are known, then

$$Q = \dot{m}_c c_{p,c} \left(T_{c,o} - T_{c,e}\right) \qquad (10)$$

The coolant mass flow $\dot{m}_c$ was kept high enough to have a fully turbulent flow ($Re \approx 7000$) with elevated heat transfer coefficient values in order to avoid any limiting heat transfer resistance in the coolant-side of the heat exchanger (bottom side).

The total amount of heat transferred is directly related to the temperature difference between the coolant and the ice slurry. Since the temperature of the coolant increases during its transport through the coiled side, the driving of the temperature difference is best expressed by the logarithmic mean temperature difference

$$\Delta T_{log} = \frac{T_{c,o} - T_{c,e}}{ln\left(\frac{T_{c,o} - T_b}{T_{c,e} - T_b}\right)} \qquad (11)$$

where during the freezing $T_b = T_f\ \omega$ (Eq. 2) (Eq. 2). The logarithmic temperature has been chosen as a characteristic parameter for each experiment, averaged along the test time.

The heat flux given by eq. 10 corresponds predominantly to the sum of the latent heat of the ice formation and the sensible heat of ice and brine. Furthermore, there is friction between scrapers and plate, and the induced flow gives rise to viscous dissipation. These two contributions represent a power input in the system, noted as Φ. Considering a time interval Δt during the ice formation process, then

$$Q = \rho_{b,0} V \left(\frac{L_f \Delta\varphi_m \big|_t^{t+\Delta t}}{\Delta t} + \frac{1-\varphi_m \;\; c_{pi} + \varphi_m c_{pb} \;\; \Delta T_b \big|_t^{t+\Delta t}}{\Delta t} \right) + \Phi \qquad (12)$$

where V is the initial brine volume in the SSPHE upper side and $\rho_{b,0}$ the brine density. Whereas the first part of eq. 12 is easily calculable from the measured temperatures, the value of Φ has not an evident definition. It can be approached assuming that the power consumed by the driving motor is all transformed into heat by viscous dissipation and friction between materials. That is obviously not true, since there are thermal and mechanical losses in the both motor and the gear box. However, for the sake of simplicity it was assumed that Φ was equal to the power measured by the wattmeter. Figure 4 shows the obtained values of Q calculated from eqs. 10 and 12. The fact that Φ is overestimated can explain the slightly higher values given by eq. 12.

The heat transfer coefficient is determined from the heat flux given by Eq. 10 and the difference between the averaged temperature of the embedded thermocouples $T_w = \overline{T}_{w,n}$ and the immersed PT100 probes $T_b = \overline{T}_{b,n}$ (Fig. 5)

$$h = \frac{Q}{A \;\; T_b - T_w} \qquad (13)$$

Once the freezing starts, the temperature difference in the above expression $T_b - T_w$ becomes equal to the wall supercooling degree ΔT_s, since $T_b = T_f$.

2.4. Experimental procedure

All the experiments were performed following the same procedure. The base brine was prepared in a separated tank, with a higher capacity than the SSPHE upper side. NaCl was added gradually to the water in the tank while it was continuously recirculated between it and the SSPHE upper side, ensuring an homogeneous NaCl concentration in all the fluid. Once the NaCl reached the 7 wt.% content the SSPHE upper side was closed. The cooling system was used then to decrease the brine temperature at 0 ºC, which was the initial temperature for all the tests. Prior to the beginning of the experiment, the coolant was cooled down to its corresponding temperature. Once the scraping speed was fixed, the pumping of the coolant to the SSPHE bottom side set the commencement of the test. Scraping speed, coolant mass flow and coolant temperature were kept constant during all the experiment. Each test took the necessary time to reach a 20% of ice content. Once this target was obtained, the slurry in the SSPHE upper side was replaced by a new volume of brine, starting again the process for the next experiment.

The experimental uncertainty was calculated by following [21]. Uncertainty calculations based on a 95% confidence level showed maximum values of 35% for the heat transfer coefficient and 37% for the Richardson number.

3. Results and discussion

3.1. Thermal response

Figure 6 presents a typical evolution of the process temperatures during a batch experiment in the SSPHE, from 0 to 20% of ice content. The process is divided in two parts: chilling and freezing. The first part, from the beginning of the experiment until the onset of nucleation corresponds to the chilling. In this stage, only sensible heat is exchanged and the brine remains liquid, with a fast decrease on the temperature T_b as a consequence. The end of this period is not only limited by the brine temperature T_b, since it reaches values lower than the freezing point. The period when the brine temperature is lower than the freezing point ($T_b < T_f$) is the so called supercooled state, where the brine is not in thermal equilibrium. The brine temperature continues decreasing during the

supercooling until the nucleation induction time t_{ni} is reached and the nucleation appears. The critical degree of supercooling and the nucleation induction time for the spontaneous nucleation on a subcooled surface is still unpredictable [9]. The temperature rises then abruptly arriving to the freezing temperature ($T_b = T_f$). The sensible heat accumulated during the supercooling is transformed into latent heat by the formation of multitude of ice crystals. This release of heat during the phase change is the responsible of the sudden temperature increase. After that, the production of ice starts, and thus the so-called freezing stage. The predominance of latent heat over the sensible heat is the responsible of the low velocity in the temperature decrease, only due to the increase of NaCl in the remaining brine.

3.2. Supercooling

The temperature pattern of the supercooling phenomenon appeared to be different from case to case, being even not reproduced by the immersed probes for some of them. This fact has been characterized by a new parameter, the supercooling amplitude ζ, defined as the amplitude of the temperature rise once the nucleation appeared (see Fig. 6).

The supercooling amplitude was found to vary directly with the scraping speed and inversely with the temperature difference between the brine and the wall $\Delta T_{b,w} = T_b - T_w$. The combination of these two factors suggests the presence of an stratified fluid layer in the bottom of the tank. In the presence of high $\Delta T_{b,w}$ or low scraping velocities the fluid layer thickness increases, leading to large temperature gradients in the SSPHE fluid. As a consequence the fluid in contact with the bottom plate would reach the maximum ζ appearing the nucleation, whereas the fluid in the upper layers (e.g. around the immersed probes) would not be yet at the freezing temperature. Moreover, large $\Delta T_{w,b}$ values imply also large wall supercooling degrees ΔT_s, which advances the nucleation. In those cases nucleation appears first on the plate and not all around the volume. The localized nucleation triggers the freezing once $T_b = T_f$, and therefore no supercooling occurs around the probes.

The experimental evidence relates the supercooling amplitude ζ with the Richardson number, which represents the ratio between forced and natural convection. Forced convection is due to the flow generated by the scrapers, playing in favour of higher ζ values. Natural convection acts against ζ, keeping the colder and therefore heavier fluid in the bottom. This phenomenon hinders the mixing and as a consequence the appearance of the nucleation in all the fluid volume. Figure 7 shows the ζ values as a function of their correspondent Richardson numbers, averaged from $T = T_f$ until the onset of nucleation, $T = T_f - \zeta$. Supercooling phenomenon was detected only for $Ri < 0.02$, with increasing values of ζ as Ri decreases. The detection of the supercooling and its amplitude ζ are therefore an indicator of the mixing level in the SSPHE.

The symbols in Figure 7 are coloured according with the nucleation induction time, defined in Fig. 6. The lack of dependence between t_{ni} and Ri can be associated with the unpredictable character of the nucleation onset. On the other hand, t_{ni} is related with ζ through the heat exchanged between the supercooled brine and the wall. If the heat flux is assumed to be time-constant, and applying eq. 13, then

$$t_{ni} \propto \zeta \frac{\rho_b V c_{p,b}}{hA\Delta T_{b,w}} \qquad (14)$$

where $\Delta T_{b,w} = T_b - T_w$ and $T_b < T_f$.

3.3. Heat transfer

Time resolved values

The evolution of the heat fluxes during the production of the ice slurry is depicted in Fig. 8 for different operating conditions (type of scraper, scraping speed and logarithmic mean temperature difference). Figures 8 and 8 correspond to two different values of ΔT_{log} , averaged during the freezing stage of the experiment (see Fig. 5), from the nucleation start until a 20% of ice content is reached. The effects of different scraper systems and scraping velocities are compared in each figure. The starting of the freezing stage can be recognized distinctively by the stabilization of the heat flux, which is a consequence of the stabilization of the process temperature. The heat transfer coefficients corresponding to the heat fluxes shown in figures 8 and 8, calculated according to Eq. 10, are represented respectively in figures 9 and 9.

• Scraper type effect

The effect of the adaptable scrapers yields a heat flux augmentation of around two times compared with the rigid scrapers, showing a slight dependency with ΔT_{log} values:larger ΔT_{log} values lead to slightly higher heat fluxes (see Fig. 8).

Regarding the heat transfer coefficient (Fig. 9), the use of the adaptable scrapers retrieves again two-fold augmentations of *h* compared to the rigid system. As opposed to the heat flux trend, heat transfer coefficients are in general slightly higher for the lowest values of ΔT_{log} value. This can be explained considering that higher supercooling degrees (ΔT_s) lead to faster growth rates, resulting in thicker ice layers on the plate surface [12].

• Scraping speed effect

In general, higher scraping velocities increase the heat flux, whereas this effect is small compared with the scraper system or the ΔT_{log} effect. The influence of the scraping speed during the freezing period is more evident on the heat transfer coefficient, which undergoes maximum increases of around 40% when *N* increases from 0.1 to 0.8 s^{-1}. Moreover, these two bounding velocities lead to two different trends, particularly noticeable with the adaptable scrapers. *h* values for *N*=0.1 s^{-1} reach a maximum when nucleation appears, after which *h* remains almost constant. On the other hand, for *N*=0.8 s^{-1} the onset of nucleation entails a sharp decrease on *h*, which reaches a maximum an instant before during the supercooling.

In spite of the similar heat fluxes observed during the freezing period, the time required to reach the 20% of ice content changed significantly with the scraping speed (see Fig. 8 and 9).These differences are attributed to the stretch of the experiments prior to the nucleation onset: faster scraping velocities provided higher heat flux values as shown in Fig. 8, advancing the freezing start respect to the low scraping speed cases.

Moreover, the higher scraping velocities ensured the presence of the supercooling phenomenon in all the brine volume. The heat released by the supercooled brine is suddenly recovered during the nucleation, where the amount of ice initially formed can be quantified by $\rho_b V c_{p,b} \zeta / L_f$. Considering a supercooling amplitude of $\zeta \approx 0.5$ ºC, the former expression gives values of around 2% of ice content. On the other hand, the lower scraping velocities do not benefit from the initially elevated heat flux values, and the nucleation onset does not represent significant values of ice content.

• Coolant temperature effect

The coolant temperature, which is the responsible of the wall supercooling degree, intensifies the different trends mentioned before. Smaller ΔT_{log} values lead to more favourable mixing situations with lower Ri and higher supercooling amplitudes ζ (see Fig. 7). Supercooling occurring all around the SSHPE volume means an immediate and uniform appearance of the nucleation, which in turn implies the absence of an ice layer on the plate before that instant. This also explains the higher *h* values obtained in these cases. Conversely, the absence of ζ indicates local nucleation on the plate, generating an ice layer that produces lower *h* values.

Although ΔT_{log} is computed as a time-averaged value, it is not constant during the experiment. The increasing NaCl content of the brine due to the ice formation leads to lower freezing temperatures, and therefore the wall supercooling degree ΔT_s undergoes a continuous decrease since the coolant temperature is kept constant. The ice formation and growth rate over the subcooled surface is then lower, being more easily removed by the scrapers. As a consequence it can be observed that the heat transfer coefficient increases with time in Fig. 8, especially for high scraping velocities and adaptable scrapers, where the scraping action is more intense.

Time-averaged values

For a better comparison between experiments, heat fluxes and heat transfer coefficients were averaged during the freezing periodas defined in Fig. 6. Figure 10 shows the time-averaged heat flux over the freezing period for different scraping velocities *N* and driving temperatures ΔT_{log} whereas figure 11 does for the time-averaged heat transfer coefficient $\overline{h}$.

• Scraper type effect

Adaptable scrapers provide a two-fold augmentation of the global heat flux compared to the rigid scrapers (Fig. 10). The difference between the two scraping systems is mainly due to the poor scraper action of the rigid scrapers. Since the scrapers are not able to follow the surface, a continuous ice layer is developed. If the presence of such an ice layer is assumed, the obtained $\overline{h}$ values will correspond to the global heat transfer coefficient $\overline{h}_T$, which includes the heat conduction through an ice layer of thickness e_i. The process side heat transfer coefficient $\overline{h}_p$ can be obtained then from,

$$\frac{1}{\overline{h}_p} = \frac{1}{\overline{h}_T} - \frac{e_i}{k_i} \quad (15)$$

If the $\overline{h}$ values of the rigid scrapers are introduced into equation 15, the resulting $\overline{h}_p$ are comparable to the $\overline{h}$ values obtained for the adaptable scrapers(see Fig. 11 and 12).

• Scraping speed effect

The scraping speed appears to have a clear but small effect on the heat transfer, that mainly depends on the logarithmic mean temperature difference. Higher scraping velocities leads to higher heat flux values. The tests where supercooling was not detected at the beginning of the freezing period (distinctively marked) correspond to low scraping velocities and indicate a poor mixing with an accumulation of ice over the subcooled surface; consequently the resulting heat fluxes are lower.

The net influence of the scraping speed on the heat transfer coefficient is represented in Fig. 12 for two different ΔT_{log} values.It is clear that the ΔT_{log} effect (which is closely related with the plate supercooling degree ΔT_s) appears to be higher than the scraping speed effect. Whereas the increase of *N* from 0.1 to 0.8 s^{-1} results in an augmentation of $\overline{h}$ of around 20%, the transition form $\Delta T_{log} = 2.4$ ℃ to 1.3 ℃ leads to a maximum augmentation of 40% for $N = 0.5$ s^{-1}.

As mentioned before, the way in which $\overline{h}$ evolves with *N* depends also on ΔT_{log}. For $\Delta T_{log} = 2.4$ ℃ *h* increases linearly with *N*. In this case the higher supercooling degree of the surface causes a thicker ice layer. This ice layer is in this case the limiting problem and thus higher scraping velocities always mean augmentations of $\overline{h}$. For $\Delta T_{log} = 1.3$ ℃ *h* decreases after $N = 0.5$ s^{-1}. In this case the scraping speed is fast enough to ensure a clean surface. The $\overline{h}$ decrease comes from the fact that $N > 0.5$ s^{-1} leads to higher ice-brine mixing situations, where the existent ice particles impact on the subcooled surface increasing the nucleation and developing an ice layer [9].

• Coolant temperature effect

Heat flux is directly proportional to augmentations on the logarithmic mean temperature difference. However, depending on ΔT_{log} the ice layer formed over the surface can alter this dependency. From figure 10 it is possible to see that the heat flux increases as ΔT_{log} increases. For the adaptable scrapers, the leap from $\Delta T_{log} \approx 1$ ℃ to $\Delta T_{log} \approx 1.5$ ℃ yields a significant augmentation compared to the further evolution, more similar to the one observed for the rigid scrapers. This similarity points to the presence of an ice layer, that even if removed by the scraper, is formed continuously: the process is driven by the particle surface impacts which in turn limit the heat transfer. Therefore the trend is similar to the one shown by the rigid scrapers (where a constant ice layer is present), but with higher heat fluxes due to the effective ice removal.

The heat transfer coefficient decreases as ΔT_{log} increases. This effect is more accentuated for the adaptable scrapers, since the increment of ΔT_{log} entails the formation of an ice layer ($\Delta T_s \propto \Delta T_{log}$); this ice layer is conversely always present for the rigid scrapers. Recalling Eq. 15, the difference between the $\bar{h}$ values for the lower and higher ΔT_{log} can be associated to the presence of an ice layer of thickness $e_i \approx 0.5$ mm (Fig. 11), which is the ice constantly formed and removed between successive scraping actions.

From Fig. 10 and 11 it is possible to deduce that even if $\bar{h}$ decreases until a minimum value for ΔT_{log} values as high as 2 ℃, at this operating condition the heat flux and therefore the ice slurry production are maximized. The decrease of $\bar{h}$ is indeed due to the higher ice production, which implies a thicker ice layer on the plate, hindering the heat transfer even if it is constantly removed. As $Q \propto h_T \cdot \Delta T_{log}$ (see Eq. 15), it is clear that the decrease on $\bar{h}$ has a lower effect than the increase of ΔT_{log}. As mentioned before, the level of ice formation on the plate is directly related with its supercooling degree ΔT_s. Figure 13 indicates that higher ΔT_{log} values implies higher ΔT_s. The higher the supercooling degree is the more nucleation occurs on the plate, and therefore it represents a thicker ice layer with lower $\bar{h}$ values.

3.4. Correlation for Nusselt number estimation

Heat transfer coefficient values have been non-dimensionalized through the Nusselt number, depicted in Fig. 14. Both Re_{rot} and Nu have been calculated based on the properties presented in Sec. 2.2. Due to the twofold effect of the ice particles (they change the rheological properties of the slurry and cause nucleation on the surface and the formation of an ice layer impacting on it), plotted results are coloured according to the product of the ice content ratio (φ_m divided by the maximum ice content of the experiment $\varphi_{m,max}$) and the Froude number: $Fr \cdot \varphi_m / \varphi_{m,max}$. This new data dimension includes the effect of the phase change and considers the effect of the ice particles in the process by accounting for their quantity φ_m and their distribution in the SSHPE. The particle distribution, which is in turn mainly affected by the buoyancy and the velocity induced by the scrapers, is weighted by the Froude number.

The results appear to be grouped according to the tested experimental conditions: $\overline{\Delta T}_s \approx 0.75$ ℃ and $\overline{\Delta T}_s \approx 1.5$ ℃. Focusing on $\overline{\Delta T}_s \approx 0.75$ ℃, the results with low ice content or high ice stratification ($\downarrow Fr$), associated with low Re_{rot} values, follow a pattern that fits with the penetration theory plus a constant term *C*, that can be related with the effect of the phase change on the subcooled surface:

$$\bar{h} = 2\sqrt{\frac{k \cdot \rho \cdot c_p \cdot n \cdot N}{\pi}} + C. \qquad (16)$$

Beyond the low effect of the ice particles in the flow (which behaves as a single phase flow), the penetration theory trend indicates that the ice particles rise after being scraped and therefore do not impact again on the subcooled surface. This absence of impacts reduce the ice formation over the surface and as a consequence the scrapers are able to remove it.

The data separate from this trend at $Re_{rot} \approx 5 \cdot 10^4$, when the product $Fr \cdot \varphi_m / \varphi_{m,max}$ approaches to 1: ice particles concentration is higher and they are better mixed. As a consequence the flow behaviour changes. Moreover the well mixed particles impact on the subcooled surface, generating the formation of an ice layer that worsens the heat transfer: the higher is $Fr \cdot \varphi_m / \varphi_{m,max}$ the lower is Nu, with a low dependence with the Re_{rot} number.

A composed correlation has been proposed to predict Nu versus Re_{rot}, Fr and φ_m for the $\overline{\Delta T}_s \approx 0.75$ ºC tests. For $Re_{rot} < 4.71 \cdot 10^4$ they have been fitted to the penetration theory plus a constant therm:

$$Nu = \left(2\sqrt{\frac{k \cdot \rho \cdot c_p \cdot n \cdot N}{\pi}} + 1200 \right) \frac{D}{k_i} = 1.53 Re_{rot}^{0.5} + 229 \qquad (17)$$

whereas for $Re_{rot} > 4.71 \cdot 10^4$ they have been fitted performing logarithmic multiple regressions to express Nu versus Re_{rot} and the product $Fr \cdot \varphi_m$:

$$Nu = 661.6 Re_{rot}^{-0.026} \; Fr\varphi_m{}^{-0.028} \qquad (18)$$

Influence of Prandtl number was also studied, showing to be insignificant. Fig. 15 presents a comparison between experimental and calculated Nusselt number values for the full range fitted, together with the regression coefficient.

The data corresponding with $\overline{\Delta T}_s \approx 1.5$ ºC show much lower Nu values. This decrease on Nu is due to the ice layer effect, as seen in Fig. 11. The high supercooling degree ΔT_s together with the initial ice particle impacts develops an ice layer of $e_i \approx 0.25$ mm, not well removed by the scrapers due to its higher level of adherence. This leads to lower values of Nu with an opposite behaviour of the $\overline{\Delta T}_s \approx 1.5$ ºC data: increases on Re_{rot} and $Fr \cdot \varphi_m / \varphi_{m,max}$ implies a more active scraping and the positive effect of the ice removal is higher than the negative effect of the ice particles impacting on the ice layer. The certain presence of the ice layer makes impractical the proposal of correlations for that values of ΔT_s.

4. Conclusions

Heat transfer phenomena during ice slurry production in a SSPHE operating in batch mode have been studied. A 7 wt. % NaCl brine was used as a base solution for the ice slurry generation. Two different scraper types, rigid and surface adaptable, were compared for different scrapers rotational speeds (0.1 s^{-1} to 0.8 s^{-1}) and coolant temperatures (ΔT_{log} from 0.5 ºC to 2.5 ºC). The major findings are as follow:

• The location of the initial nucleation in the SSPHE was found to depend on the Richardson number. The effects of buoyancy, supercooling degree and forced velocities effect interact leading to an initial localized nucleation over the subcooled plate ($Ri > 0.02$) or to a global fluid volume nucleation ($Ri < 0.02$). The detected supercooling amplitude was found to be a good indicator of the fluid mixing inside the SSPHE upper side.

• The configurations with adaptable scrapers shown a better performance in the ice slurry generation and heat transfer, avoiding the presence of no-scraped regions and effectively removing the formed ice layer. Augmentations on the heat transfer coefficient of around two times were found with respect to the rigid scraper.

• The rotational speed of the scrapers was found to have a low effect on the heat transfer, influenced by the supercooling degree of the surface. Maximum averaged heat fluxes of 1000 W/m^2 and averaged heat transfer coefficients of 4000 W/m^{2}K were found for the adaptable scrapers with surface supercooling degrees of ≈ 0.5 ºC.

• Heat transfer results were non-dimensionalized by means of the Nusselt and Re_{rot} numbers. Low supercooling degree values adopted the shape of the penetration theory for low Re_{rot} values, whereas at high values Nu becomes almost independent of Re_{rot} (Nu =550), mostly due to the impact of the particle over the surface at higher mixing rates. Higher surface supercooling degrees led to a constant ice layer that reduced the Nu values to ≈ 350.

• A correlation was proposed for a supercooling degree of 0.75 ºC composed by the penetration theory plus a constant therm for $Re_{rot} < 4.71 \cdot 10^4$ and a correlation based on Re_{rot} and $Fr \cdot \varphi_m$ for $Re_{rot} > 4.71 \cdot 10^4$, with global $R^2 = 0.87$.

References

[1] P. Zhang and Z. Ma, "An overview of fundamental studies and applications of phase change material slurries to secondary loop refrigeration and air conditioning systems," *Renewable and Sustainable Energy Reviews*, vol. 16, no. 7, pp. 5021 – 5058, 2012.

[2] C. S. Rao and R. W. Hartel, "Scraped surface heat exchangers," *Critical Reviews in Food Science and Nutrition*, vol. 46, no. 3, pp. 207–219, 2006.

[3] H. Abichandani, S. Sharma, and D. Heldman, "Hydrodynamics and heat transfer in liquid full scraped surface heat exchanger –a review," *Journal of Food Process Engineering*, vol. 9, pp. 121–141, 1987.

[4] R. Cuevas and M. Cheryan, "Heat transfer in a vertical, liquid-full scrapedsurface heat exchanger. application of the penetration theory and wilson plots models [relevant to food processing]," *Journal of Food Process Engineering*, vol. 5, pp. 1–21, 1982.

[5] P. Harriot, "Heat transfer in scraped surface heat exchangers," *Chem. Eng. Prog. Symp. Ser*, vol. 29, pp. 137–139, 1959.

[6] A. H. Skelland, D. R. Oliver, and S. Tooke, "Heat transfer in a water-cooled scraped-surface heat exchanger," *Brit. Chem. Eng*, vol. 7, pp. 346–353, 1962.

[7] F. G. Qin, X. D. Chen, and A. B. Russell, "Heat transfer at the subcooled-scraped surface with/without phase change," *AIChE Journal*, vol. 49, no. 8, pp. 1947–1955, 2003.

[8] F. G. Qin, J. C. Zhao, A. B. Russell, X. D. Chen, J. J. Chen, and L. Robertson, "Simulation and experiment of the unsteady heat transport in the onset time of nucleation and crystallization of ice

from the subcooled solution," *International Journal of Heat and Mass Transfer*, vol. 46, no. 17, pp. 3221–3231, 2003.

[9] F. G. Qin, A. B. Russell, X. D. Chen, and L. Robertson, "Ice fouling on a subcooled metal surface examined by thermo-response and electrical conductivity," *Journal of Food Engineering*, vol. 59, no. 4, pp. 421–429, 2003.

[10] R. J. C. Vaessen, M. M. Seckler, and G. J. Witkmap, "Heat transfer in scraped eutectic crystallizers," *International Journal of Heat and Mass Transfer*, vol. 47, no. 4, pp. 717–728, 2004.

[11] R. Vaessen, C. Himawan, and G. Witkamp, "Scale formation of ice from electrolyte solutions on a scraped surface heat exchanger plate," *Journal of Crystal Growth*, vol. 237–239, Part 3, no. 0, pp. 2172–2177, 2002.

[12] F. G. Qin, X. D. Chen, and K. Free, "Freezing on subcooled surfaces, phenomena, modeling and applications," *International Journal of Heat and Mass Transfer*, vol. 52, no. 5–6, pp. 1245–1253, 2009.

[13] M. B. Lakhdar, R. Cerecero, G. Alvarez, J. Guilpart, D. Flick, and A. Lallemand, "Heat transfer with freezing in a scraped surface heat exchanger," *Applied Thermal Engineering*, vol. 25, no. 1, pp. 45–60, 2005.

[14] F. G. Qin, X. D. Chen, S. Ramachandra, and K. Free, "Heat transfer and power consumption in a scraped-surface heat exchanger while freezing aqueous solutions," *Separation and Purification Technology*, vol. 48, no. 2, pp. 150 – 158, 2006.

[15] E. Stamatiou, J. Meewisse, and M. Kawaji, "Ice slurry generation involving moving parts," *International Journal of Refrigeration*, vol. 28, no. 1, pp. 60 – 72, 2005.

[16] A. Melinder, *Thermophysical properties of liquid secondary refrigerants*. International Institute of Refrigeration, 1997.

[17] R.H. Perry, D. Green, *Perry's Chemical Engineer's Handbook*. fifth edition, McGraw-Hill, New York, 1973.

[18] V. Ayel, O. Lottin, and H. Peerhossaini, "Rheology, flow behaviour and heat transfer of ice slurries: a review of the state of the art," *International Journal of Refrigeration*, vol. 26, no. 1, pp. 95–107, 2003.

[19] A. Kitanovski, D. Vuarnoz, D. Ata-Caesar, P. W. Egolf, T. M. Hansen, and C. Doetsch, "The fluid dynamics of ice slurry," *International Journal of Refrigeration*, vol. 28, no. 1, pp. 37–50, 2005.

[20] D.G. Thomas, "Transport characteristics of suspension," *J. Colloid. Sci.*, vol. 20, pp. 267–277, 1965.

[21] R. J. Moffat, “Describing the uncertainties in experimental results,” *Experimental Thermal and Fluid Science*, vol. 1, no. 1, pp. 3 – 17, 1988.

Parameter	Value	Parameter	Value
H	0.1 m	ω_0	7 wt. %
H_S	3.9 cm	N	0.1–0.8 s^{-1}
D	0.610 m	ΔT_{log}	0.5–2.5 °C
A	0.29 m^2	Re_c	≈ 7000
n	4	Re_{rot}	$350–1.4 \cdot 10^5$

Table 1: Dimensions and operating conditions for the heat transfer characterization

Figure captions

Figure 1: Schematic view of the experimental facility

Figure 2: Images of different sections inside the SSPHE

(a) Coolant channels under the subcooled plate

(b) Adaptable scrapers

Figure 3: Adaptable scraper system (left), thermocouples distribution (center) and welding technique (right)

Figure 4: Calculated heat fluxes for the coolant and ice slurry sides along time

Figure 5: Cross sectional schematic view with ice slurry, wall and coolant temperatures

Figure 6: Representative case of the evolution of the process temperature along time

Figure 7: Supercooling amplitude ζ for different Ri numbers

Figure 8: Heat fluxes on the subcooled plate along the test duration for different $\overline{\Delta T}_{log}$ values

(a) $\overline{\Delta T}_{log} = 1.3$ °C

(b) $\overline{\Delta T}_{log} = 2.4$ °C

Figure 9: Heat transfer coefficient on the subcooled plate along the test duration for different $\overline{\Delta T}_{log}$ values

(a) $\overline{\Delta T}_{log} = 1.3$ °C

(b) $\overline{\Delta T}_{log} = 2.4$ °C

Figure 10: Influence of $\overline{\Delta T}_{log}$ on the heat flux averaged over the freezing period. Results coloured by scraping velocity

Figure 11: Influence of $\overline{\Delta T}_{log}$ on the heat transfer coefficient averaged over the freezing period. Results coloured by the scraping velocity

Figure 12: Influence of the scraping velocity on the heat transfer coefficient averaged over the freezing period for different scrapper systems and $\overline{\Delta T}_{log}$ values

Figure 13: $\overline{\Delta T}_{log}$ *vs.* $\overline{\Delta T}_{s}$ coloured by the heat transfer coefficient (adaptable scrapers)

Figure 14: Nusselt (Nu) number vs. rotating Reynolds (Re_{rot}) number for different experiments (adaptable scrapers)

Figure 15: Comparison between experimental and calculated Nusselt number values

Parameter	Value	Parameter	Value
H	0.1 m	ω_0	7 wt. %
H_S	3.9 cm	N	0.1–0.8 s^{-1}
D	0.610 m	ΔT_{log}	0.5–2.5 °C
A	0.29 m^2	Re_c	≈7000
n	4	Re_{rot}	350–1.4·10^5

Table 1: Dimensions and operating conditions for the heat transfer characterization

Figure captions

Figure 1: Schematic view of the experimental facility

Figure 2: Images of different sections inside the SSPHE

(a) Coolant channels under the subcooled plate (b) Adaptable scrapers

---

Figure 3: Adaptable scraper system (left), thermocouples distribution (center) and welding technique (right)

Figure 4: Calculated heat fluxes for the coolant and ice slurry sides along time

---

Figure 5: Cross sectional schematic view with ice slurry, wall and coolant temperatures

Figure 6: Representative case of the evolution of the process temperature along time

---

Figure 7: Supercooling amplitude ζ for different Ri numbers

Figure 8: Heat fluxes on the subcooled plate along the test duration for different $\overline{\Delta T}_{log}$ values

(a) $\overline{\Delta T}_{log}$ =1.3 °C (b) $\overline{\Delta T}_{log}$ =2.4 °C

Figure 9: Heat transfer coefficient on the subcooled plate along the test duration for different $\overline{\Delta T}_{log}$ values

(a) $\overline{\Delta T}_{log}$ =1.3 °C (b) $\overline{\Delta T}_{log}$ =2.4 °C

Figure 10: Influence of $\overline{\Delta T}_{log}$ on the heat flux averaged over the freezing period. Results coloured by scraping velocity

---

Figure 11: Influence of $\overline{\Delta T}_{log}$ on the heat transfer coefficient averaged over the freezing period. Results coloured by the scraping velocity

Figure 12: Influence of the scraping velocity on the heat transfer coefficient averaged over the freezing period for different scrapper systems and $\overline{\Delta T}_{log}$ values

Figure 13: $\overline{\Delta T}_{log}$ *vs.* $\overline{\Delta T}_{s}$ coloured by the heat transfer coefficient (adaptable scrapers)

Figure 14: Nusselt (Nu) number vs. rotating Reynolds (Re_{rot}) number for different experiments (adaptable scrapers)

Figure 15: Comparison between experimental and calculated Nusselt number values

Figure 1

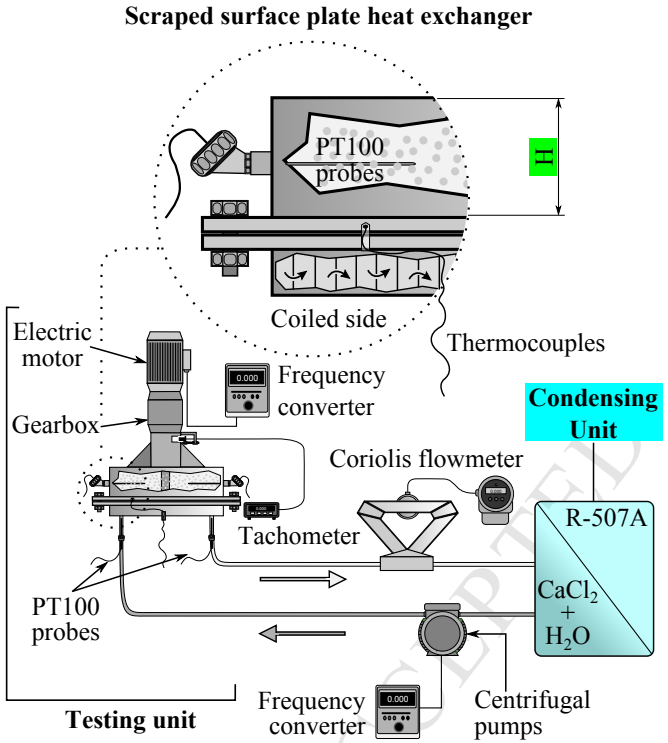

Figure 2a

Click here to download high resolution image

Figure 2b

Click here to download high resolution image

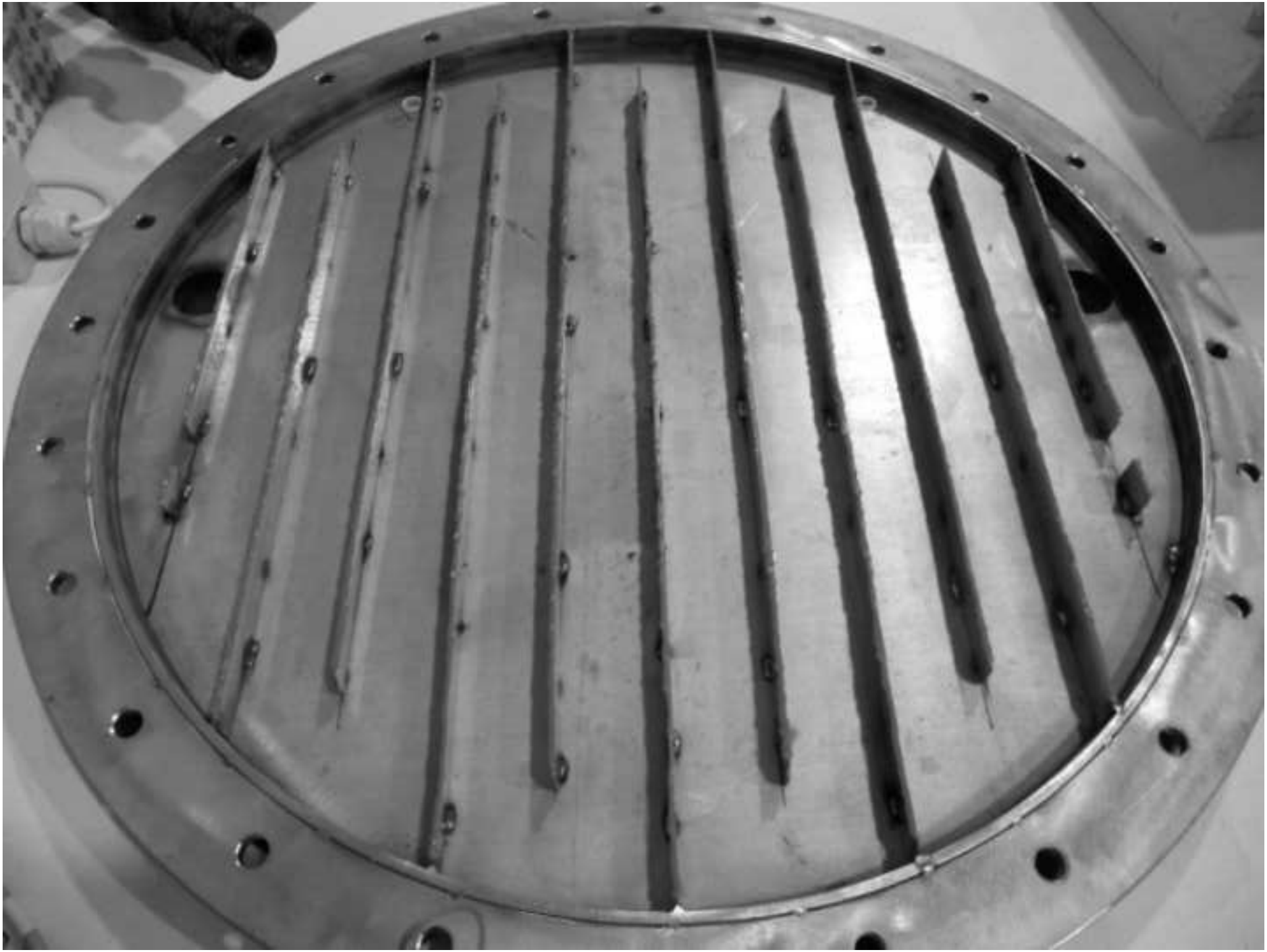

Figure 3

Click here to download high resolution image

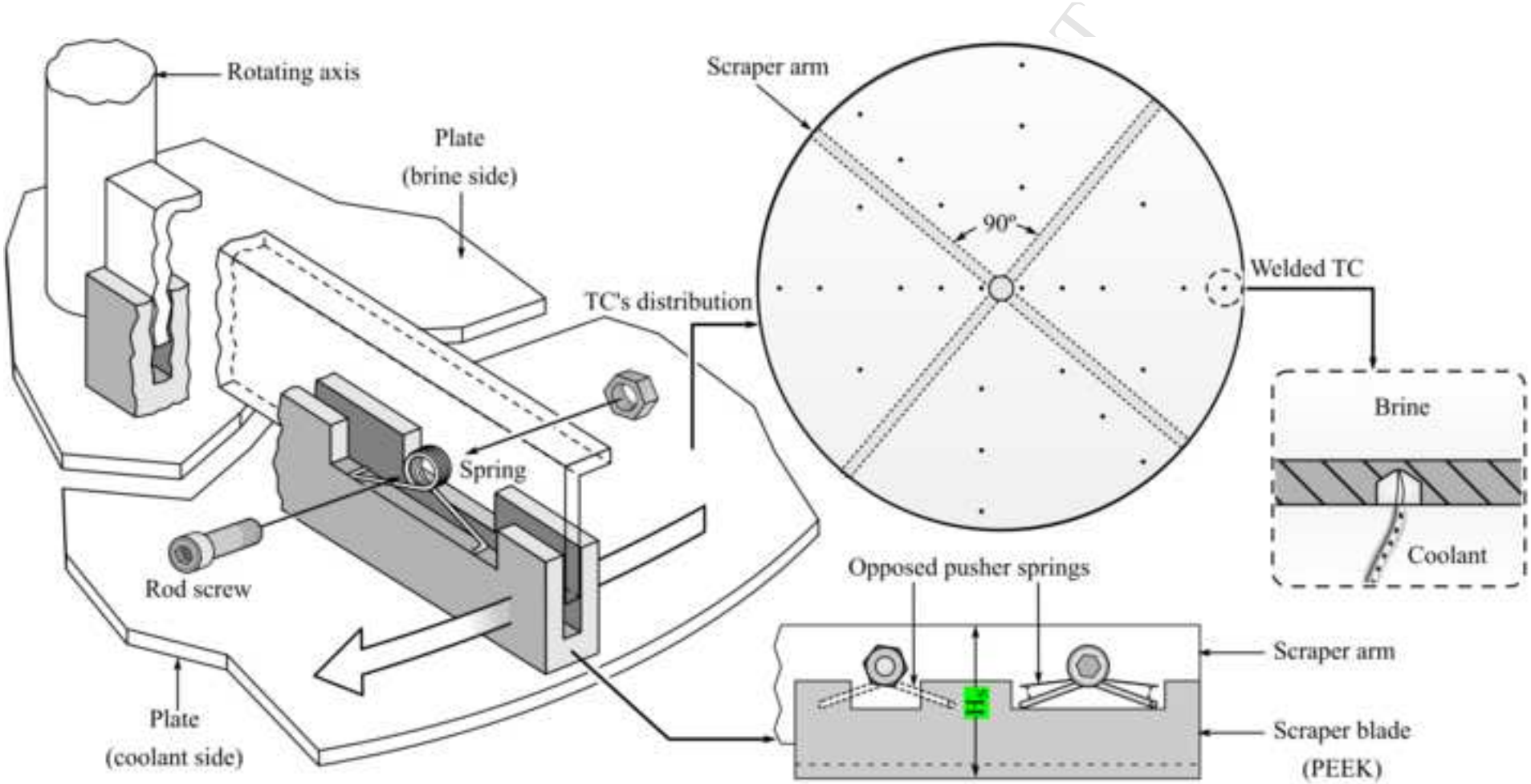

Figure 4

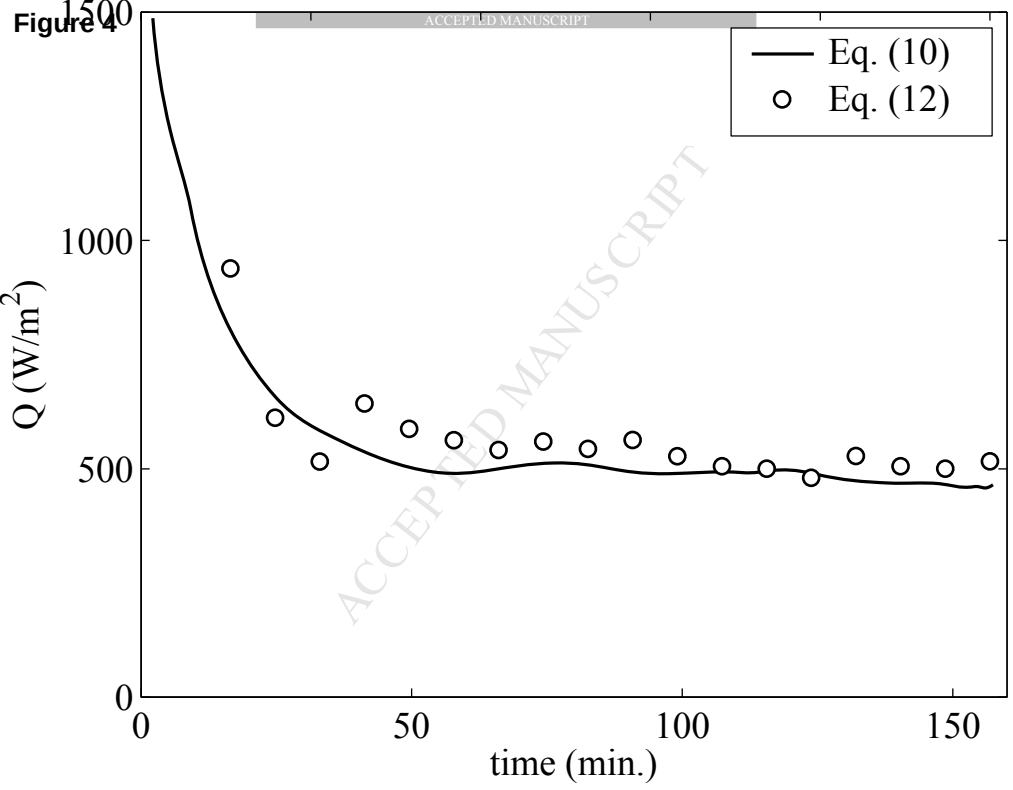

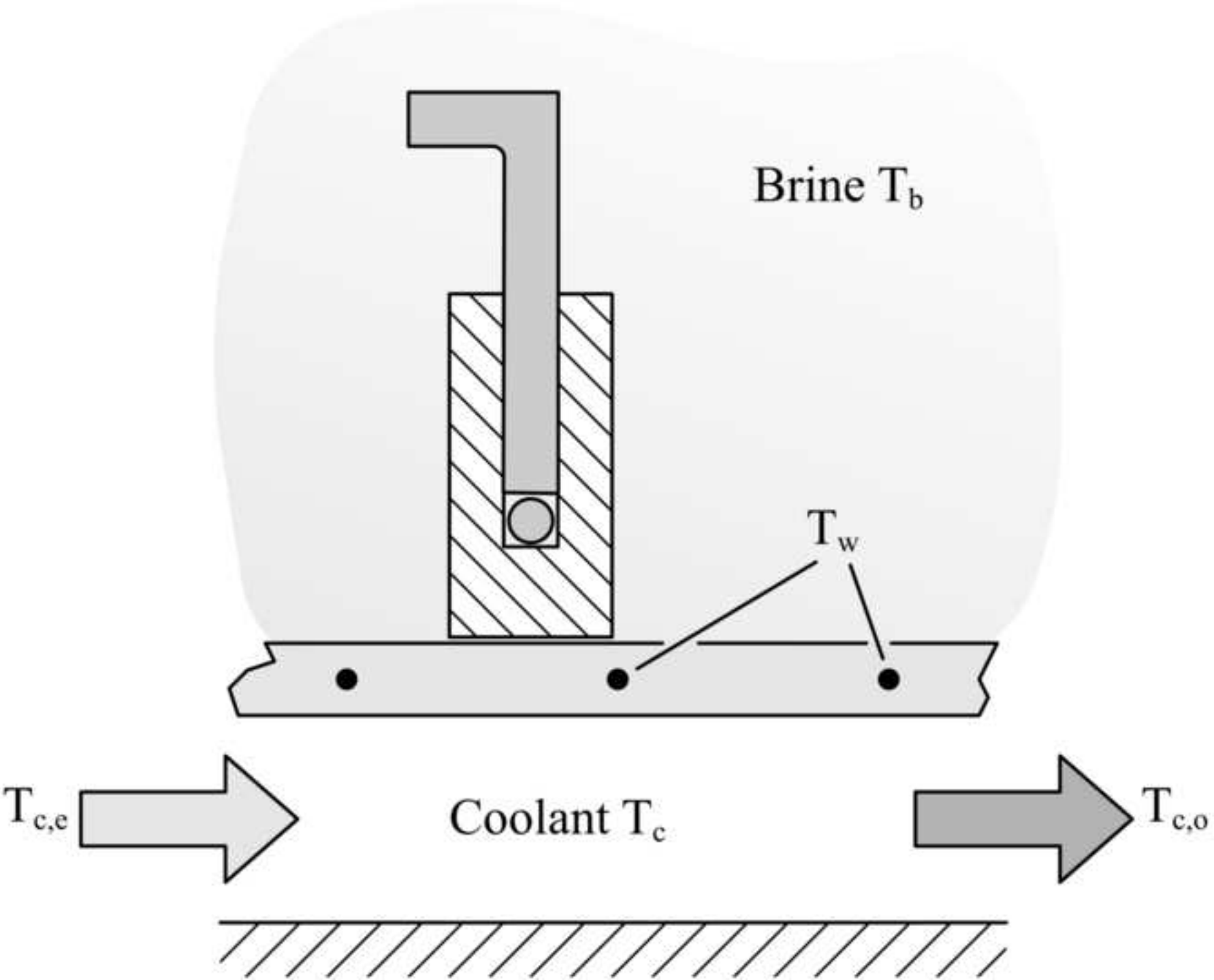

Figure 6

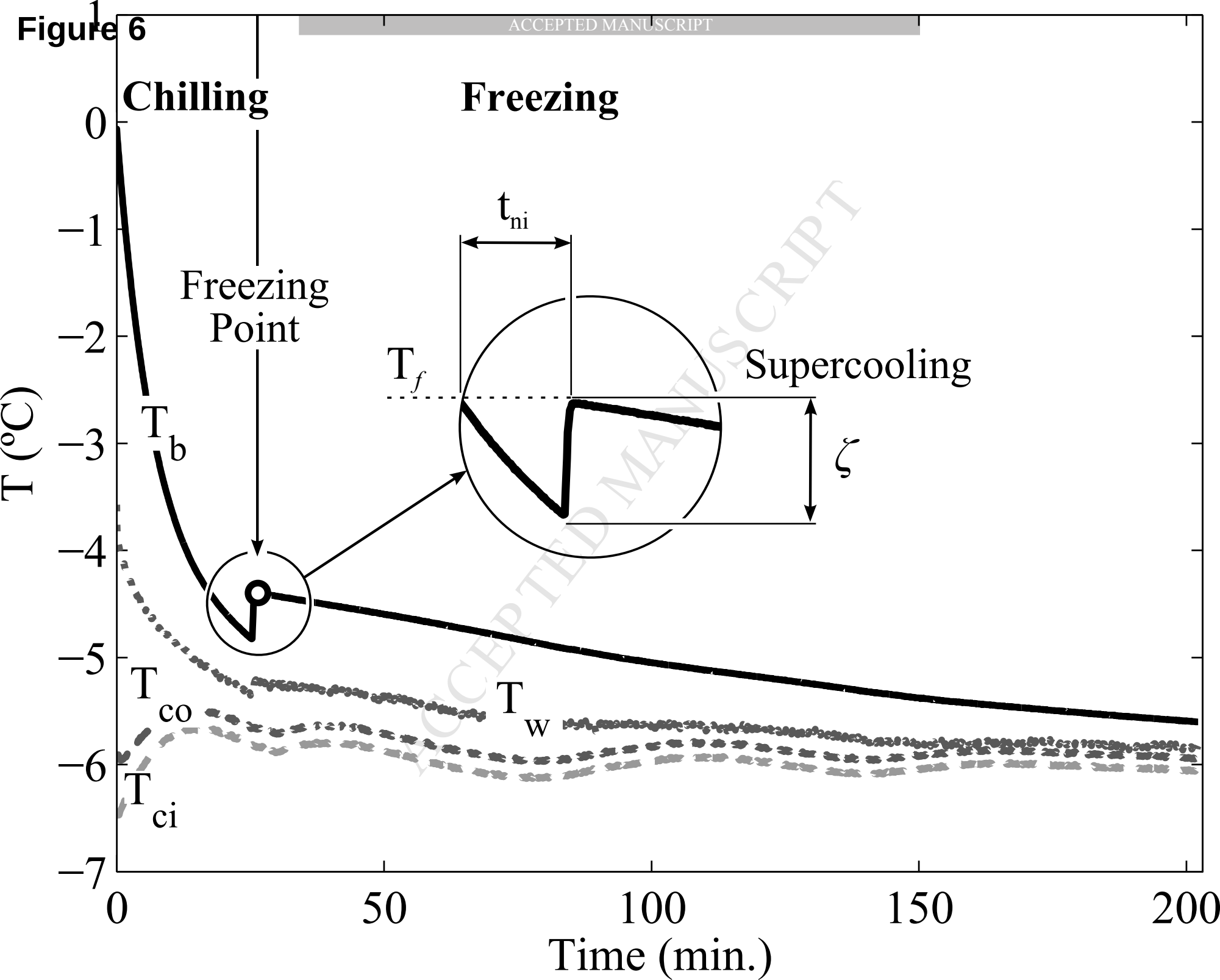

Figure 7

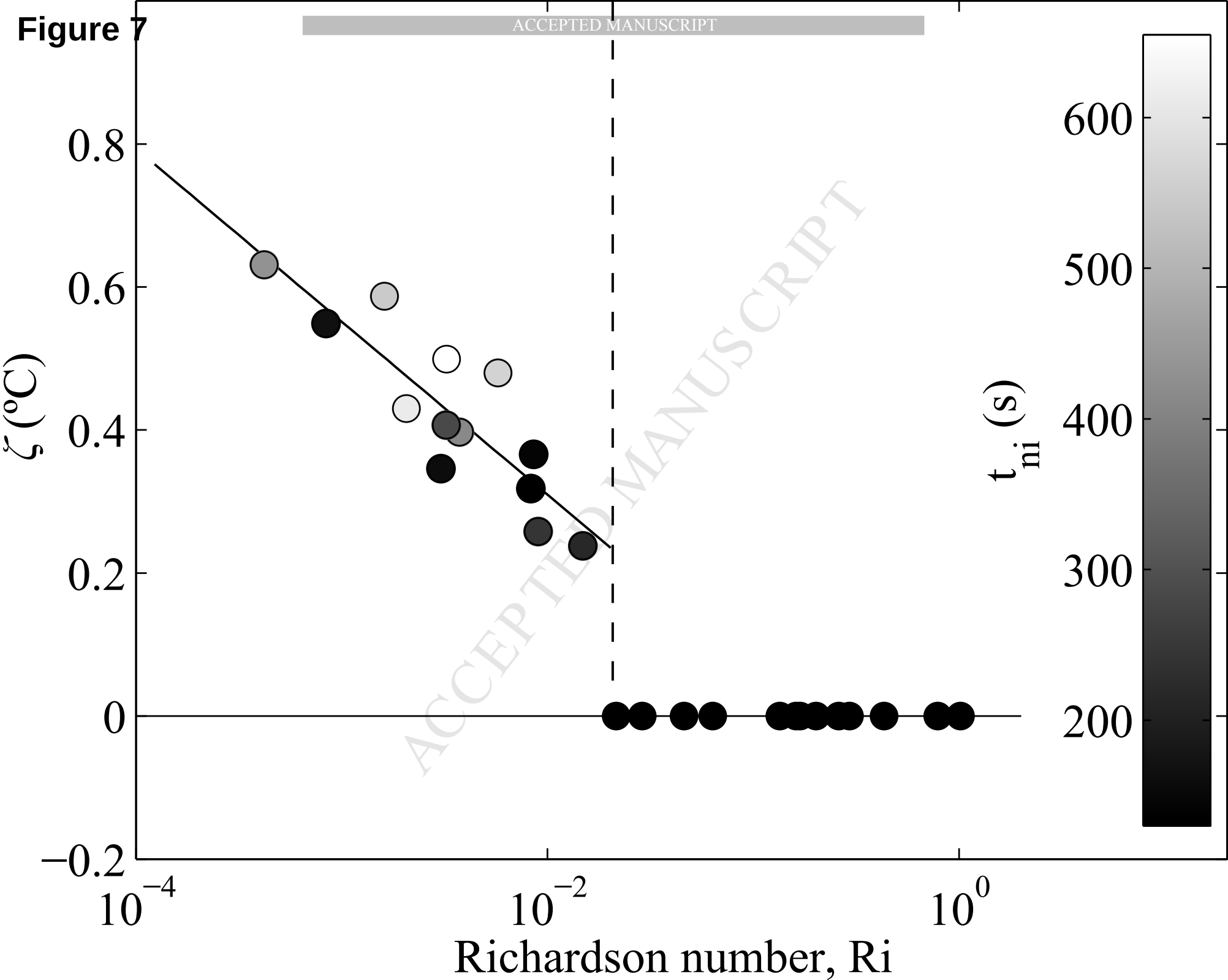

Figure 8a

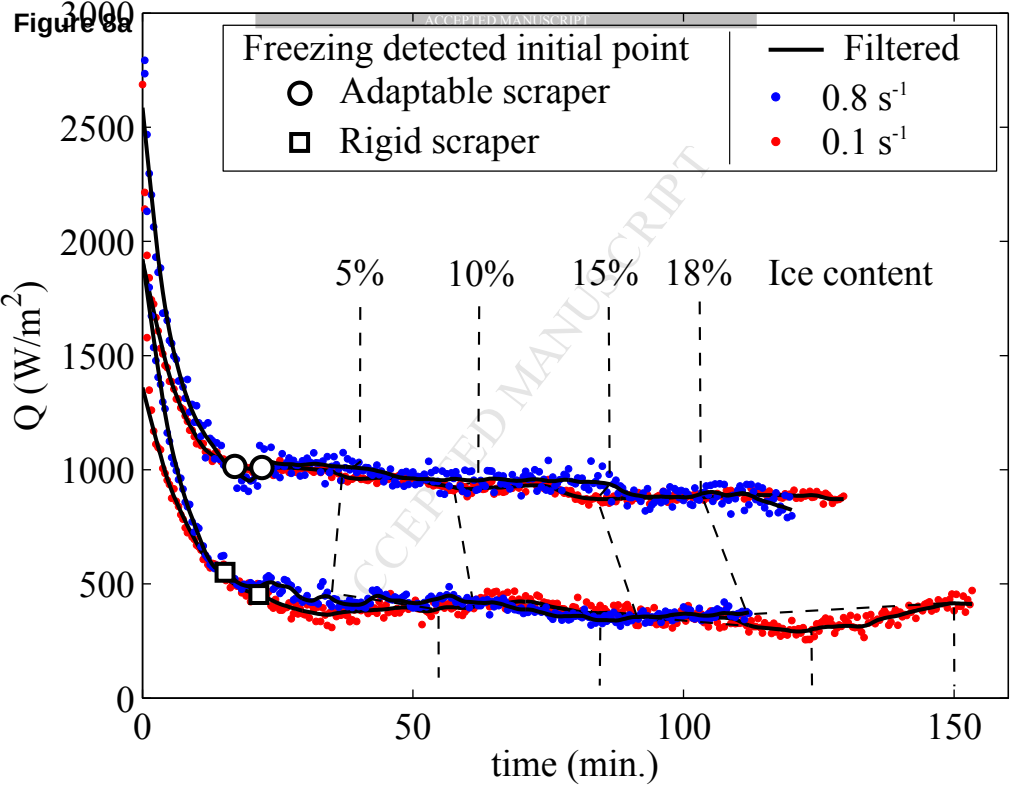

Figure 8b

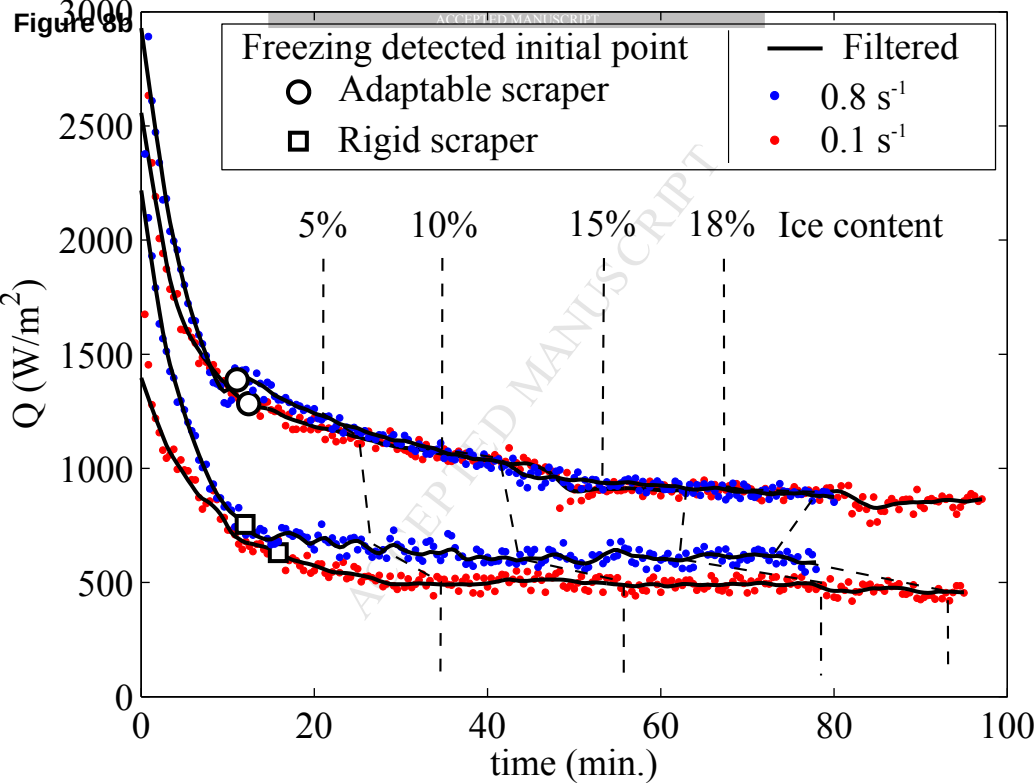

Figure 9a

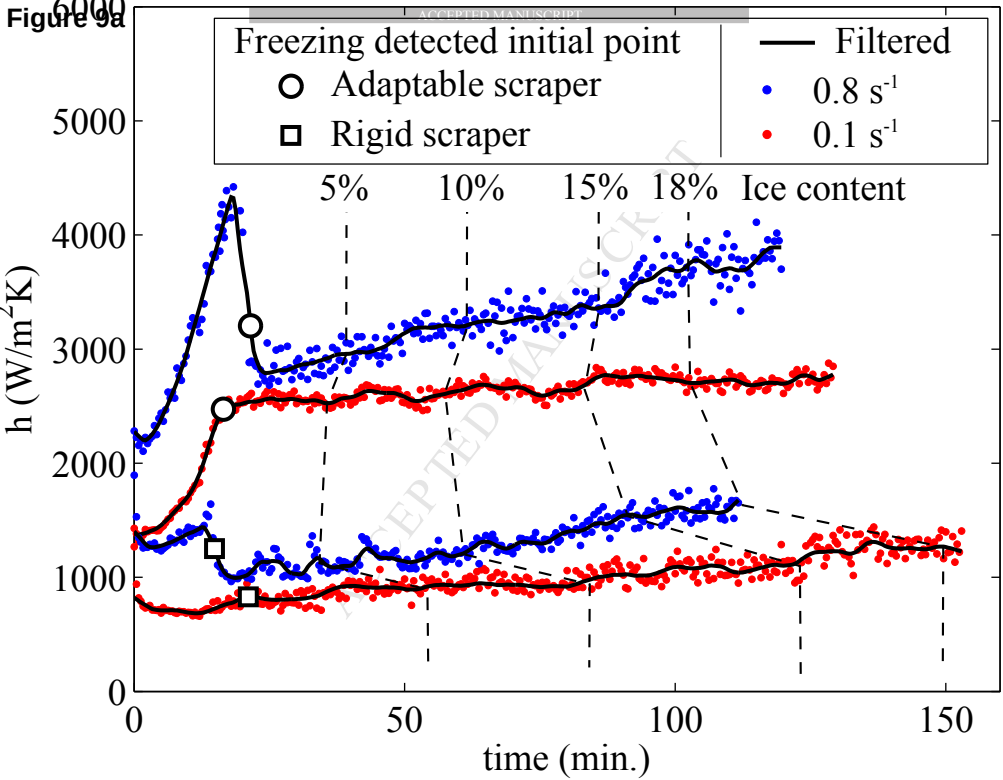

Figure 9b

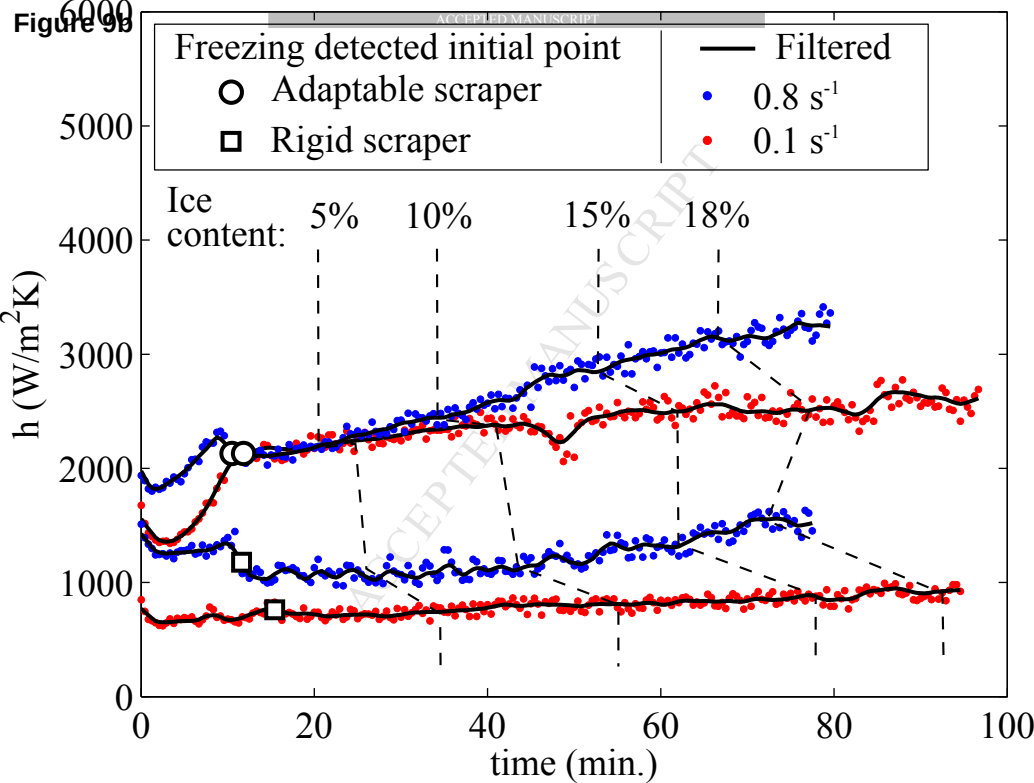

Figure 10

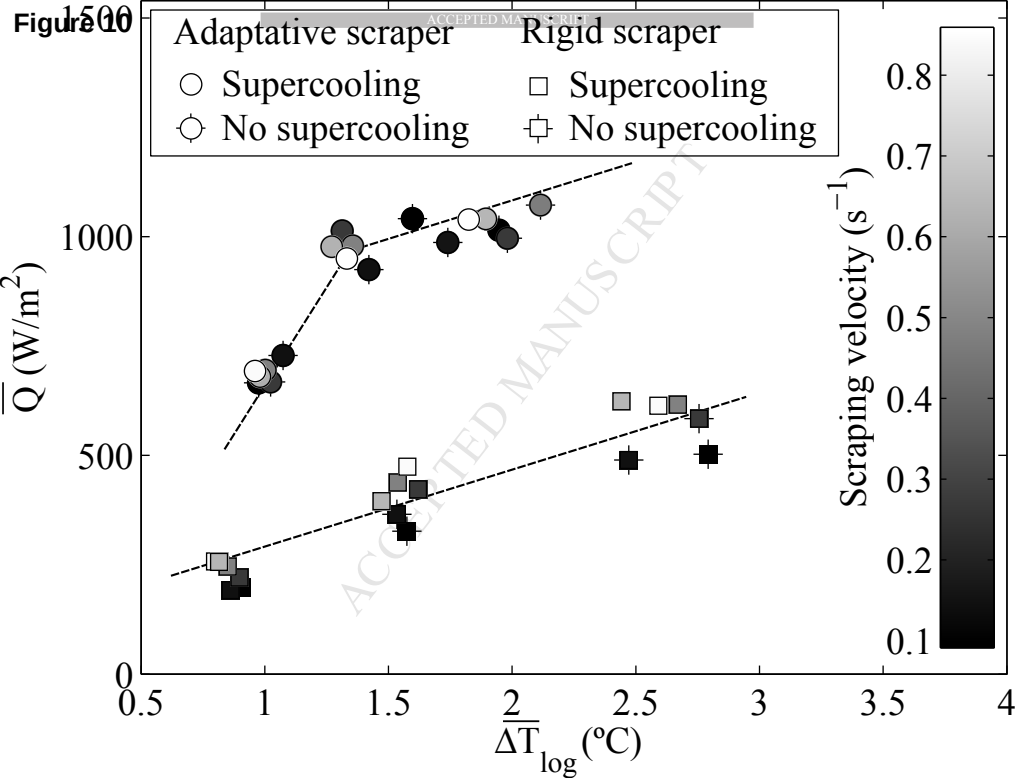

Figure 11

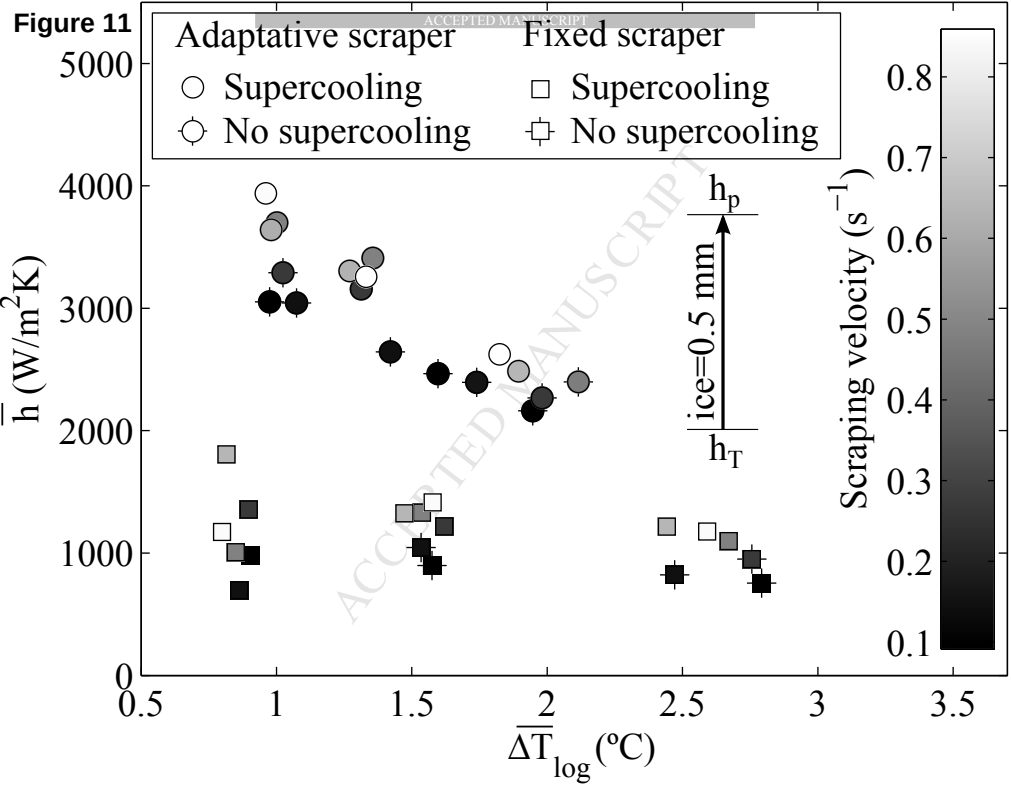

Figure 12

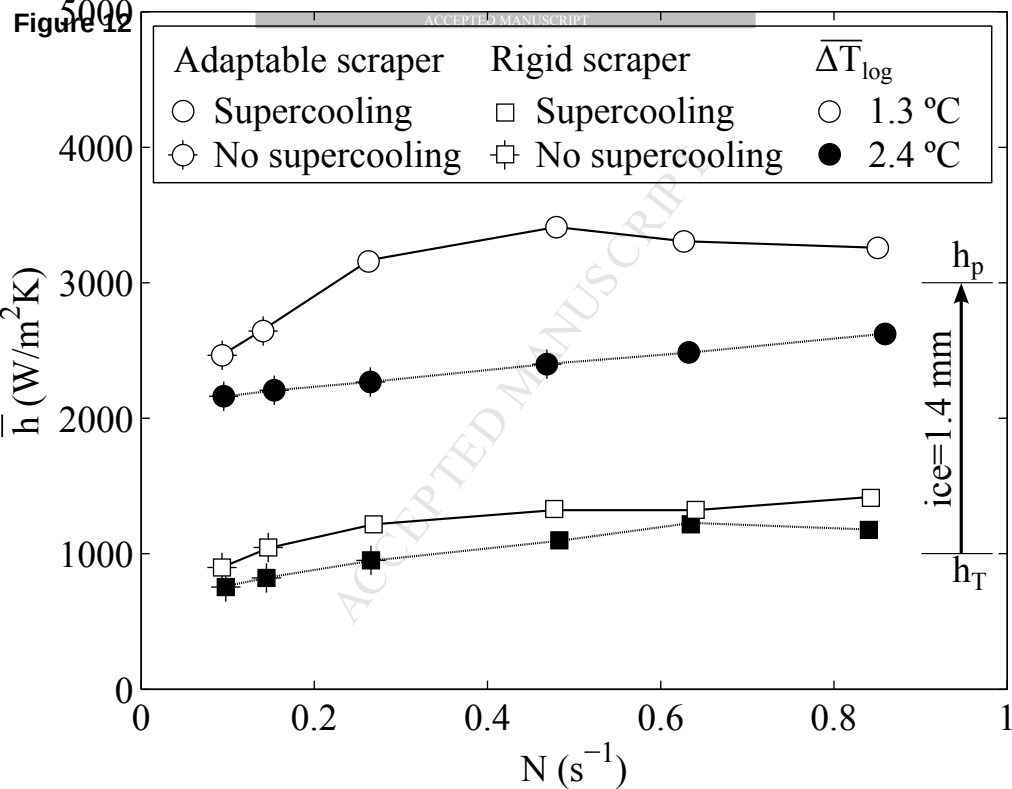

Figure 13

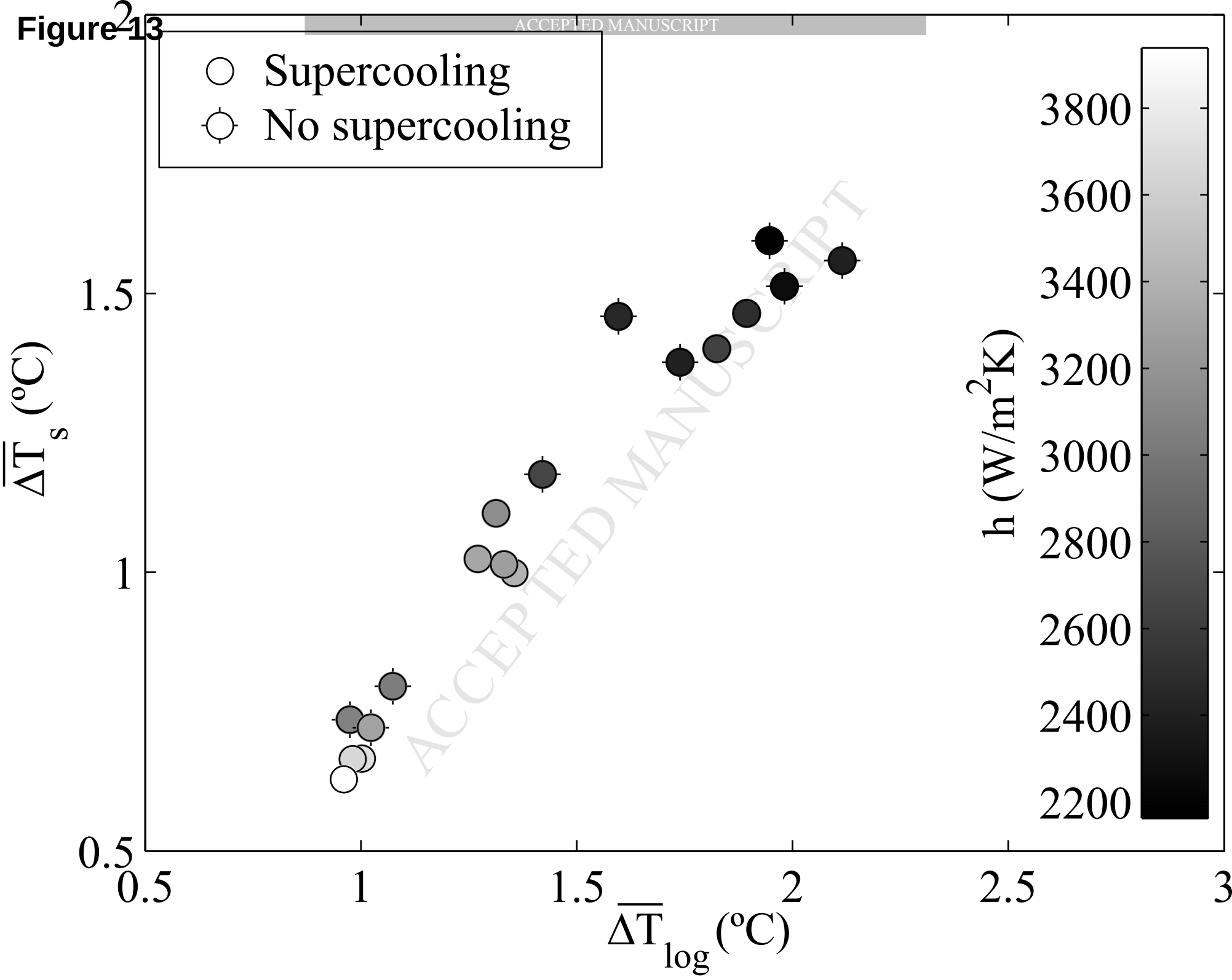

Figure 14

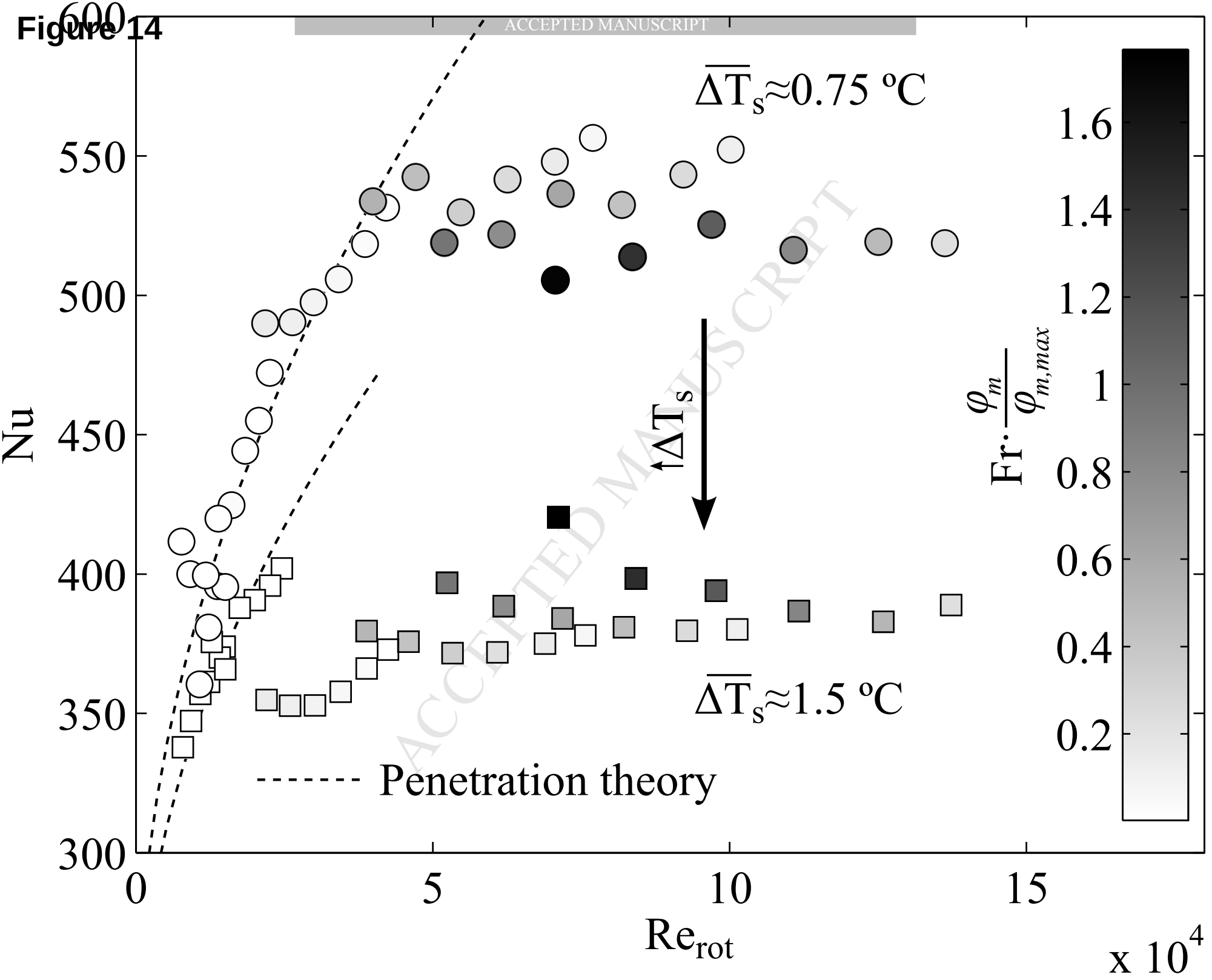

Figure 15